Soft route for monodisperse Gold nanoparticles confined within -SH functionalized walls of mesoporous silica.

Eric Besson, Ahmad Mehdi, Catherine Reyé, Robert J. P. Corriu

Soft route for monodisperse gold nanoparticles confined within SH-functionalized walls of mesoporous silica†

Eric Besson, Ahmad Mehdi,* Catherine Reyé and Robert J. P. Corriu

Received 6th February 2009, Accepted 23rd April 2009
First published as an Advance Article on the web 28th May 2009
DOI: 10.1039/b902568e

In this paper, we report a soft route leading to small gold nanoparticles confined within the framework of 2D-hexagonal mesoporous SH-functionalised silicas. For that purpose, a hydrophilic bis-silylated precursor containing a disulfide unit was prepared. Framework-functionalised materials were obtained in one step by the "direct synthesis" method which consists of a co-hydrolysis and polycondensation of a bridged organosilica precursor with tetraethylorthosilicate (TEOS) in the presence of a non-ionic triblock co-polymer (P123) as structure-directing agent. Reduction of SS groups leads quantitatively to SH functional groups within the framework of 2D hexagonal mesoporous silicas. All these materials have been characterised by TEM, ^{13}C and ^{29}Si NMR experiments, nitrogen gas adsorption, powder XRD and elemental analysis. The subsequent growth of monodisperse gold nanoparticles of small size ($\sim$2 nm) within the walls of mesoporous materials was studied and is discussed.

Introduction

In recent years, metal nanoparticles have attracted much attention because of the unique dependence of their physical and chemical properties on their size. This is attributed to the quantum confinement phenomenon as well as the high ratio of surface to bulk atoms.[1] Therefore, the preparation of monodisperse metal nanoparticles (NPs) is a significant challenge. One approach consists of using the regular pore channels of ordered mesoporous silica as matrixes for controlling the growth and organisation of nanoparticles.[2] This strategy is based on weak interactions between the inner silica surface and the metal precursors with as the consequence of the possible migration of NPs on the outer surface. Thus, by this approach, the metal dispersion and the NP size distribution depend on the nature of the metal, the reaction conditions and the metal loading. To overcome these drawbacks, several groups[3] and some of us[4] used ordered and functionalised mesoporous silica as nanoreactor to obtain metal nanoparticles of controlled size. The procedure was generally based on metallic precursor impregnation onto the mesoporous organosilica with subsequent reduction/decomposition of the metal precursor to generate the nanoparticles. Thanks to the appropriate functional groups incorporated within the channel pores of the mesostructured materials, the anchoring of the metal precursor then occurs exclusively within the internal surface of the material by stronger interactions between the metal and the functional groups. This methodology avoids the growth of nanoparticles on the external surface, which would involve a broad particle size distribution. Furthermore, by changing the functional group/metal precursor ratio, it is possible to control the metal loading as well as the nanoparticle size.

Institut Charles Gerhardt, Chimie Moléculaire et Organisation du Solide, Université Montpellier, cc 1701. Place E. Bataillon, 34095 Montpellier Cedex 5, France. E-mail: ahmad.mehdi@univ-montp2.fr; Fax: +33 4 6714 3852; Tel: +33 4 6714 3038

† Electronic supplementary information (ESI) available: Additional graphs and figures. See DOI: 10.1039/b902568e

While a number of reports concern the location of NPs in the channel pores of mesoporous silica, there are only some papers relating to the selective location of NPs in the walls of mesoporous materials. Garcia *et al.* described the incorporation of γ-Fe_2O_3 nanoparticles in the walls of aluminosilicates.[5] For that purpose, they used a block-copolymer-based "one-pot" self-assembly approach followed by calcination of the composite at 750 °C. Yuranov *et al.* described an approach leading to PdNPs in the micropores of SBA-15 thanks to an ion-exchange reaction followed by an H_2 reduction of the composite at 300 °C.[6] Yang *et al.* reported a method for the selective functionalisation of the surfaces of the meso- and micropores of SBA-15 and the subsequent deposition of metal NPs within the micropores of this type of bimodal porous material.[7]

The location of NPs in the framework of mesoporous materials leaving the mesopores empty is a great challenge. Indeed, such materials could open routes to new materials containing, for example, two kinds of NP perfectly located at nanometric scale, one in the channel pores and the other in the framework. This will involve the design of materials with novel properties.

With the view to investigate the properties of such materials, we devised a new and soft method allowing the location of NPs in the wall of ordered mesoporous organosilica, without any thermal treatment .

Our approach is based on the functionalisation of the framework of mesoporous organosilica with an appropriate organic group followed by the impregnation/reduction of an organometallic compound. The specific interactions between the metal and the functional group determine the location of NPs in the walls. It is worth noting that a study regarding AuNPs in the framework of mesoporous silica based on the same approach as us was made at the same time as ours.[8]

The first step of our method is the preparation of a periodic mesoporous organosilica, in which the organic fragments are located and covalently linked within the framework. Periodic mesoporous organosilica (PMOs) described for the first time in 1999 are formed by hydrolytic polycondensation of bridged

silsesquioxanes of general formula $[(RO)_3Si]_mR'$ ($m \geq 2$) in the presence of a structure-directing agent.[9] A large number of papers concerning materials obtained from at least a bis-silylated organosilane or by co-condensation of at least a bis-silylated organosilane with tetraethyl orthosilicate (TEOS) have been reported due to the great interest of functionalising the framework to tailor the properties of mesoporous silica.[10–14]

However, the introduction of functional groups able to modify the chemical or physical properties into the framework of a mesoporous material remains a challenge. Indeed, the main limitation to the formation of PMOs (even those obtained by co-condensation with TEOS) is that some precursors of general formula $[(RO)_3Si]_mR'$ ($m \geq 2$) do not give rise to periodic mesoporous materials. Some others can give rise to ordered materials but in which the organic fragments are not always located in the framework. This could be due either to the lack of rigidity of some organic precursors and/or to their poor hydrophilic character.[15,16] Both of these parameters restrict considerably the type of organic groups able to be incorporated in PMOs. Furthermore, it appears that the determination of the location of organic groups (pores or framework) is not always easy. Thus, the materials prepared from bis[3-(triethoxysilyl)propyl]tetrasulfide (TESPTS) illustrate the difficulties which can be encountered starting from bridged silsesquioxanes: Li *et al.*[17] synthesized MCM-41-type mesoporous organosilicas with tetrasulfide "embedded in the framework" *via* the co-condensation of TESPTS and tetramethoxysilane (TMOS). They noticed that mesoporous organosilicas synthesized with TESPTS/TMOS molar ratios in the range 1:8 to 1:3 have extensive structural defect holes in the nanochannels. Two years later, they reported[18] the preparation of organosilica by co-condensation of TESPTS and TMOS in the presence of P123 as a structure-directing agent. By changing the TESPTS/TMOS molar ratio, they observed that TESPTS can act as both a swelling agent and a co-agent for the formation of a microemulsion with surfactant micelles, leading to mesophase transformations. This suggests the location of the tetrasulfide moieties in the core of the micelles. In another study reported[19] at the same time, the location of tetrasulfide moieties was depicted in the pore channels. These examples highlight the difficulty of determining the location of some kinds of functional groups within mesoporous organosilica.

In this paper, we describe a route leading to the preparation of 2D hexagonal mesoporous silicas containing SS groups within the framework. We show that the transformation of SS groups into SH groups allows the confinement of monodisperse gold nanoparticles (AuNPs) of small size (~2 nm) in the walls of mesoporous materials. AuNPs were chosen, as their properties in particular as catalyst are strongly dependent on their size.[20] We show that the location of AuNPs within the framework of the 2D hexagonal mesoporous organosilicas requires the presence of SH groups.

Experimental

General procedures

The triblock copolymer ($PEO_{20}PPO_{70}PEO_{20}$ with PEO = poly(ethylene oxide) and PPO = poly(propylene oxide)) Pluronic 123, 2,2′-diaminediethyldisulfide hydrochloride salt, tetraethylorthosilicate (TEOS) and triphenylphosphine were purchased from Aldrich and used as supplied. 3-Isocyanatopropyltriethoxysilane was purchased from ABCR. Hydrogen tetrachloroaurate(III) hydrate was purchased from Strem. Chloro(tetrahydrothiophene)gold(I) (AuCl(THT)) was synthesized as described in the literature.[21] Both the CP-MAS ^{29}Si and ^{13}C solid-state NMR spectra were recorded on a BRUKER FTAM 300, in the latter case by using the TOSS technique. The repetition time was 5 s (for ^{13}C) and 10 s (for ^{29}Si) with contact times of 3 ms (for ^{13}C) and 5 ms (for ^{29}Si). The duration of the ^1H pulse was 4.2 μs (for ^{13}C) and 4.5 μs (for ^{29}Si) and the MAS rate was 10 kHz (for ^{13}C) and 5 kHz (for ^{29}Si). Chemical shifts (δ, ppm) were referenced to Me_4Si (^{13}C and ^{29}Si). Q^n and T^n notations are given respectively for $((SiO)_nSiO_{4-n})$ and $R(SiO)_nSiO_{3-n})$ environments. Specific surface areas were determined by the Brunauer-Emmett-Teller (BET) method on a Micromeritics Tristar 3000 analyser (using 74 points and starting from 0.01 as value for the relative pressure) and the average pore diameters were calculated by the BJH method. Powder X-ray diffraction patterns were measured on a Bruker D5000 diffractometer equipped with a rotating anode (Institut Européen des Membranes, Montpellier, France). Transmission electron microscopy (TEM) observations were carried out at 100 kV on a JEOL 1200 EXII microscope. Samples for TEM measurements were prepared using ultramicrotomy techniques and then deposited on copper grids. Elemental analyses of Si, C, N, S, and Au were performed by the Service Central d'Analyse (CNRS, Vernaison, France). The UV-visible diffuse reflectance spectra (Kubelka-Munk units) were measured with a Perkin Elmer Lambda 35 UV/Vis spectrophotometer equipped with a reflectance attachment. The reference used was $BaTiO_3$, and the measurements were achieved without dilution of the samples.

Synthesis of bis-silylated precursor 2

A suspension of cystamine dihydrochloride (2.20 g, 9.77 mmol) in methylene chloride (CH_2Cl_2) was briefly treated with a solution of NaOH (1 M). The aqueous phase was extracted three times with CH_2Cl_2 and the collected organic phases were dried over $MgSO_4$. The solvent was removed under vacuum yielding 1.3 g (87%) of cystamine. 3-Isocyanatopropyltriethoxysilane (4.27 g, 17.28 mmol) was added to a milky solution of cystamine (1.3 g, 8.55 mmol) in THF in a Schlenk tube under argon. The temperature increased and the solution became clear; it was kept stirred at room temperature overnight. Then the solvent was removed, and the crude product was taken up in pentane (50 mL). After filtration, precursor **2** was obtained quantitatively as a white powder. Mp: 108 °C. ^1H NMR (δ_{ppm}, 200 MHz, d_6-DMSO): 0.53 (4H, t, $^2J_{H-H} = 8.7$ Hz), 1.16 (18H, t, $^3J_{H-H} = 6.9$ Hz), 1.42 (4H, m), 2.75 (4H, t, $^3J_{H-H} = 6.7$ Hz), 2.96 (4H, q, $^3J_{H-H} = 6.1$ Hz), 3.29 (4H, q, $^3J_{H-H} = 6.1$ Hz), 3.76 (12H, q, $^3J_{H-H} = 6.9$ Hz), 6.06 (2H, t, $^3J_{H-H} = 5.5$ Hz).^{13}C NMR (δ_{ppm}, 50 MHz, d_6-DMSO): 7.7, 18.7, 24.0, 38.8, 38.9, 42.5, 58.2, 158.4. ^{29}Si NMR (δ_{ppm}, 40 MHz, d_6-DMSO): −45.6. SM (FAB+, NBA): m/z = 647 [MH^+] (40%), 601 [M − EtO] (100%).

Synthesis of materials X_n2

All the materials $\mathbf{X_n2}$ were prepared according to the same procedure. They were named $\mathbf{X_n2}$; **X** indicates Xerogel, **2** specifies the organosilica precursor and **n** corresponds to the TEOS/S molar ratio in the initial mixture. The preparation of $\mathbf{X_{20}2}$ is given as an example.

$\mathbf{X_{20}2}$. In a typical synthesis procedure, 1.57 g of P123 ($EO_{20}PO_{70}EO_{20}$) was dissolved at 30 °C in 47 mL of an 2 M aqueous HCl solution and 8 mL of water. 3.23 g (15.53 mmol) of TEOS and a solution of **2** (0.25 g, 0.39 mmol) in EtOH (1 mL) were then added under stirring. The resulting mixture was stirred at 30 °C for 24 h and then kept at 110 °C for 48 h. The surfactant was removed by hot ethanol extraction in a Soxhlet apparatus over 24 hours. After filtration and washing with EtOH, 0.94 g (86%) of $\mathbf{X_{20}2}$ was obtained as a white powder. ^{13}C CP-MAS NMR (δ, 75 MHz): 8.68, 22.02, 41.43, 159.36; ^{29}Si CP-MAS NMR (δ, 60 MHz): −65.74 (T^3), −101.60 (Q^3), −110.09 (Q^4); Anal. calcd. C 9.21, H 1.53, N 3.58, S 4.09, Si 37.59. Found C 7.95, H 1.33, N 3.10, S 3.55, Si 38.80. S_{BET} 549 m^2g^{-1}; D_p 5.4 nm; V_p 0.75 cm^3g^{-1}.

All the materials $\mathbf{X_nSH}$ were prepared according to the same procedure. They were named $\mathbf{X_nSH}$, in which **SH** specifies the thiol group. The preparation of $\mathbf{X_{20}SH}$ is given as an example.

$\mathbf{X_{20}SH}$. In a typical procedure, triphenylphosphine (0.10 g, 0.39 mmol) was added to a suspension of $\mathbf{X_{20}2}$ (0.50 g, 0.28 mmol of SS groups) in a mixture of dioxane (1.1 mL) and water (0.3 mL). The mixture was heated at 40 °C and two drops of concentrated hydrochloric acid was added. The resulting suspension was then stirred at 40 °C under argon for 2 hours (until the triphenylphosphine/triphenylphosphine oxide ratio no longer changes by ^{31}P NMR spectroscopy). After filtration and washing with EtOH and acetone, 0.49 g of $\mathbf{X_{20}SH}$ was obtained as a white powder. ^{13}C CP-MAS NMR (δ, 75 MHz): 8.19, 20.81, 21.54, 41.92, 159.36; ^{29}Si CP-MAS NMR (δ, 60 MHz): −65.74 (T^3), −101.60 (Q^3), −110.09 (Q^4); S_{BET} 593 m^2g^{-1}; D_p 5.4 nm; V_p 0.80 cm^3g^{-1}.

Materials with gold nanoparticles $\mathbf{X_nAu_m}$ were prepared according to the same procedure. They were named $\mathbf{X_nAu_m}$, **m** corresponding to the Au/S molar ratio × 100 in the initial mixture. Preparation of $\mathbf{X_{20}Au_5}$ is given as an example.

$\mathbf{X_{20}Au_5}$. A suspension of $\mathbf{X_{20}SH}$ (300 mg) in tetrahydrofuran (THF, 20 mL) was placed in a Schlenk tube immersed in an oil bath at 60 °C. A solution of AuCl(THT) (10 mg, 0.074 mmol) in THF (5 mL) was then added, followed 15 min later by addition of a solution of Na(acac)·H_2O (5 mg, 0.089 mmol) in THF (5 mL). Addition of Na(acac) results in the formation of the unstable complex Au(acac)(THT), which reacts immediately with thiol groups to give the polymeric complex (Au^ISR). The resulting suspension was stirred for a further 15 min and filtered off. The white solid (305 mg) obtained was vacuum-dried at 120 °C for 12 h. A 200 mg portion of the impregnated material was suspended in 20 mL of ethanol, and a 5 mL aliquot of a freshly prepared solution of $NaBH_4$ in ethanol (0.132 M) was added. The resulting pinkish suspension was stirred in an oil bath at 60 °C for 12 h. The solution was filtered off, and the brown solid obtained was vacuum-dried at 120 °C for 12 h to give $\mathbf{X_{20}Au_5}$.

Results and discussion

1. Preparation and characterisation of ordered and framework SH-functionalised mesoporous silicas

First, we attempted to prepare a 2D hexagonal silica containing SS groups within the framework by co-condensation of bis[3-(triethoxysilyl)propyl] disulfide **1** and tetraethyl orthosilicate (TEOS) in the presence of P123 as structure-directing agent.[22] As we intended to introduce AuNPs within the framework of mesoporous materials after reduction of SS groups into SH groups, it was of importance to obtain a well-structured 2D hexagonal material to prove their location. Unfortunately, whatever the experimental conditions (weakly[21] and strongly[23] acidic media, as well as preformed lyotropic liquid crystal phases as the structure-directing agents[24]), small-angle X-ray scattering (SAXS) patterns of the resulting materials exhibited only a single broad diffraction peak characteristic of a wormlike structure. At this stage, we decided to use a more hydrophilic bis-silylated precursor containing disulfide group in the core. For that purpose, we prepared the precursor **2** by reaction between 3-isocyanatopropyltriethoxysilane and 2,2′-diaminediethyldisulfide in THF (Scheme 1). Compound **2** was quantitatively obtained and fully characterized by ^{1}H, ^{13}C and ^{29}Si NMR spectroscopies (see experimental section).

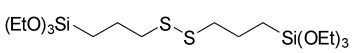

1

Mesoporous materials containing disulfide units were then prepared by co-condensation of **2** and TEOS in the presence of P123 as template (Scheme 2) under experimental conditions inspired from those described by Jaroniec.[22] The materials obtained were named $\mathbf{X_n2}$ with **n** = 10, 20 and 40 indicating the TEOS/sulfur atom molar ratio in the initial mixture.

The ^{29}Si CP-MAS NMR spectra of the materials $\mathbf{X_{10-40}2}$ are very similar. The spectrum of $\mathbf{X_{10}2}$ is given as an example in Fig. 1. It exhibited three signals at −65.2, −102.0 and −110.0 ppm assigned to T^3 ($RSi(OSi)_3$), Q^3 ($Si(OSi)_3(OH)$) and Q^4

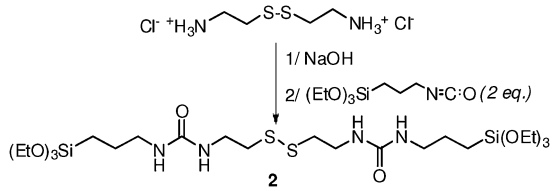

2

Scheme 1 Preparation of bis-silylated hydrophilic precursor **2**.

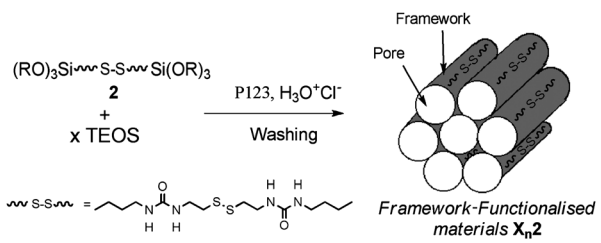

Scheme 2 Preparation of materials $\mathbf{X_{10}2}$, $\mathbf{X_{20}2}$ and $\mathbf{X_{40}2}$.

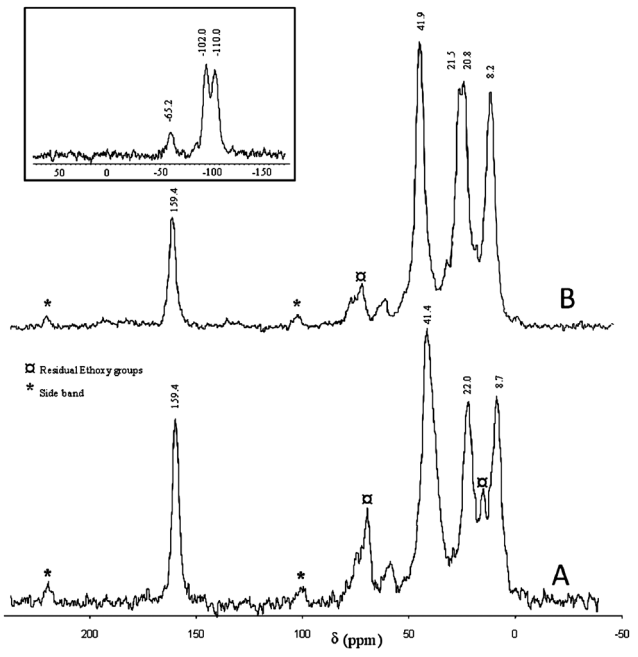

Fig. 1 ^{13}C CP-MAS NMR spectra of materials $\mathbf{X_{10}2}$ (A) and $\mathbf{X_{10}SH}$ (B). The inset shows the ^{29}Si CP-MAS NMR spectrum of $\mathbf{X_{10}2}$.

($Si(OSi)_4$) substructures respectively, indicating that the material is well condensed. The presence of a signal attributed to the T^3 substructure implies that the organic moieties were covalently bonded to the inorganic silicate framework.

The ^{13}C CP-MAS NMR spectra of the materials $\mathbf{X_{10-40}2}$ were very similar. The spectrum of $\mathbf{X_{10}2}$ is given as an example in Fig. 1. This revealed that the organic units remained intact during the sol-gel process, as indicated by the resonances at 8.7 and 159.4 ppm, resonances which are attributed to the CH_2Si and C(O)NH carbon atoms respectively.

The composition of the final materials was inferred from the results of Si, N and S elemental analyses, which were found to be close to those of the original mixtures (Table 1).

The N_2 adsorption–desorption measurements at 77 K for $\mathbf{X_{10}2}$, $\mathbf{X_{20}2}$ and $\mathbf{X_{40}2}$ showed type IV isotherms with a clear H_1-type hysteresis loop at relative high pressure, characteristic for mesoporous materials (Fig. 2). The BET surface areas were in the range of 350 to 600 $m^2\ g^{-1}$, the total pore volumes of 0.48 to 0.90

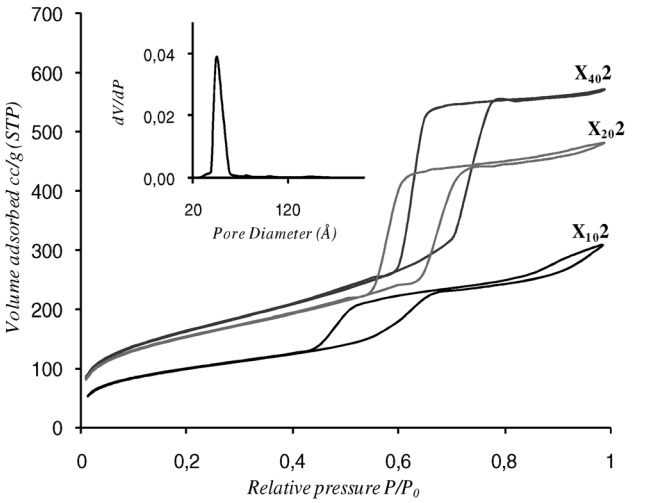

Fig. 2 N_2 adsorption–desorption isotherms for $\mathbf{X_{40}2}$, $\mathbf{X_{20}2}$ and $\mathbf{X_{10}2}$. The inset shows the pore size distribution for $\mathbf{X_{20}2}$ determined from the desorption branch of the isotherm.

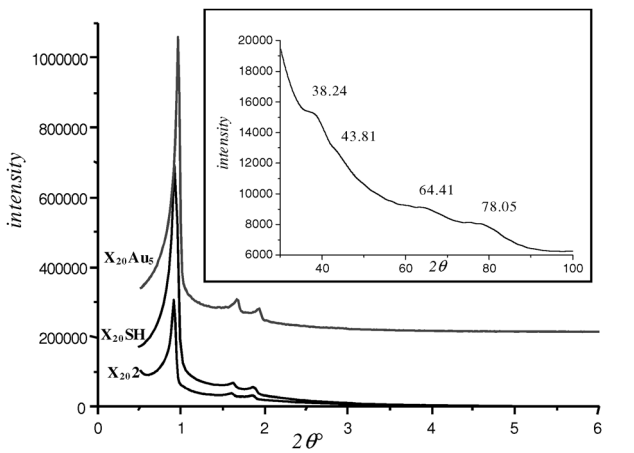

Fig. 3 X-Ray diffraction patterns of $\mathbf{X_{20}2}$, $\mathbf{X_{20}SH}$ and $\mathbf{X_{20}Au_5}$. The inset shows the pattern of Au nanoparticles.

$cm^3\ g^{-1}$ and the pore size distributions were narrow (Table 1). It is worth noting that, for materials with high content in organic groups, the isotherms are not completely reversible at high P/P_0.

Table 1 Composition and physicochemical characteristics of the materials $\mathbf{X_{10}2}$, $\mathbf{X_{20}2}$ and $\mathbf{X_{40}2}$ containing SS groups and the corresponding materials $\mathbf{X_{10}SH}$, $\mathbf{X_{20}SH}$ and $\mathbf{X_{40}SH}$

Material	Si/S [a]	S/N [a]	S_{BET} ($m^2\ g^{-1}$)	V_p ($cm^3\ g^{-1}$)	D_p (nm) [b]	a_0 (nm) [c]	d_{100} (nm)	Wall thickness (nm) [d]
$\mathbf{X_{10}2}$	13.3 (10.5)	0.45 (0.5)	357	0.48	5.3	9.55	8.27	4.25
$\mathbf{X_{20}2}$	25.4 (21)	0.45 (0.5)	549	0.75	5.4	10.92	9.46	5.52
$\mathbf{X_{40}2}$	38.8 (41)	0.56 (0.5)	593	0.88	5.9	10.66	9.23	4.76
$\mathbf{X_{10}SH}$	13.3 (10.5)	0.45 (0.5)	500	0.66	5.3	9.80	8.49	4.50
$\mathbf{X_{20}SH}$	25.4 (21)	0.45 (0.5)	593	0.80	5.4	11.04	9.56	5.64
$\mathbf{X_{40}SH}$	38.8 (41)	0.56 (0.5)	621	0.92	5.9	11.45	9.92	5.55

[a] Calculated from elemental analyses. [b] Calculated from the desorption branch by the BJH method. [c] Lattice spacing. [d] Calculated by a_0 − pore size ($a_0 = 2d_{100}/3^{1/2}$). Theoretical values are in parentheses.

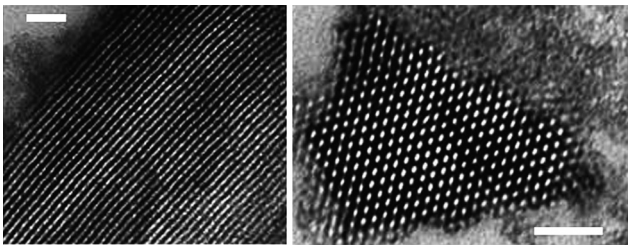

Fig. 4 TEM images of $\mathbf{X_{20}2}$. Scale bars: 50 nm.

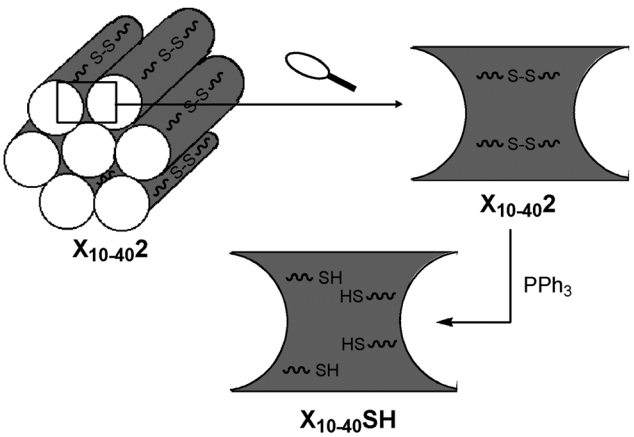

Fig. 5 Reduction of SS into SH groups.

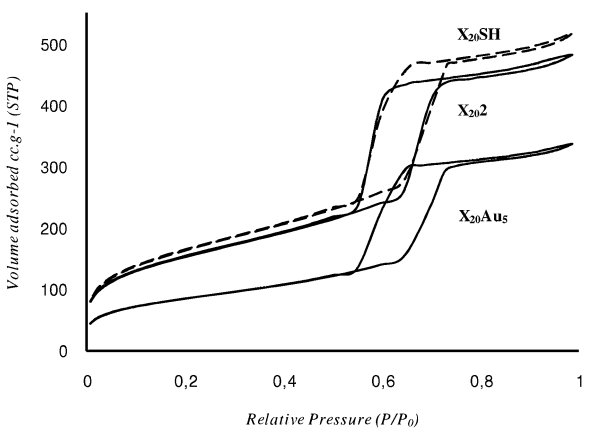

Fig. 6 N_2 adsorption–desorption isotherms for $\mathbf{X_{20}2}$, $\mathbf{X_{20}SH}$ and $\mathbf{X_{20}Au_5}$.

The X-ray diffraction (XRD) patterns of materials $\mathbf{X_n2}$ exhibit three low-angle diffraction peaks, characteristic of well ordered SBA-15 type materials (See ESI 1†). The XRD pattern of $\mathbf{X_{20}2}$ is given as an example in Fig. 3.

Further evidence for a highly ordered hexagonal structure was provided by transmission electron microscopy images (Fig. 4).

The quantitative reduction of disulfide units was achieved by treatment of materials $\mathbf{X_{10–40}2}$ with a solution of triphenylphosphine[25] giving rise to materials named $\mathbf{X_{10–40}SH}$ (Fig. 5). The ^{13}C CP-MAS NMR spectra of the resulting materials were very similar. The spectrum of $\mathbf{X_{10}SH}$ is given as an example in Fig. 1. The appearance of a resonance around 21 ppm attributed to CH_2SH is in accordance with the expected chemical transformation. The composition of materials was inferred from the results of C, N and S elemental analyses (Table 1). The N_2 adsorption–desorption isotherms for $\mathbf{X_{10–40}SH}$ (See ESI 2†) are analogous to those of the starting materials, except that for $\mathbf{X_{10}SH}$ in which a notable increase of the surface area was observed. The isotherm of $\mathbf{X_{20}SH}$ is given as an example in Fig. 6.

Interestingly, the XRD patterns of the materials $\mathbf{X_{10–40}SH}$ showed that the hexagonal structure was maintained after chemical modification (See ESI 3†). The pattern of $\mathbf{X_{20}SH}$ is given as an example in Fig. 3.

2. Preparation of gold nanoparticles within mesoporous organosilicas $\mathbf{X_{10–40}SH}$

AuNPs within the materials $\mathbf{X_{10–40}SH}$ were prepared in two steps (Fig. 7) according to the procedure which we have previously described.[4a] It consists of anchoring chloro(tetrahydrothiophene)gold(I) [AuCl(THT)] as organogold precursor within the materials $\mathbf{X_{10–40}SH}$ thanks to SH groups. This step involves the formation of an $(–Au^{I}SR)_p$ polymer.[26] The colorless solids were then treated with an ethanolic sodium borohydride ($NaBH_4$) solution, providing after filtration and drying pale brown composite materials named $\mathbf{X_{10–40}Au_m}$ (**m** indicating the Au/S ratio × 100 in the initial mixture) (see experimental section). It is worth noting that we used Au/S ratio less than 0.5 for all cases. Indeed, when we prepared AuNPs within the channel pores of mesoporous materials containing mercaptopropyl groups, we observed that for Au/S ≥1, there is outer pore growth of NPs.[4a] This was attributed to an excess of organogold precursor which could not be stabilized by thiol groups, giving rise to the formation of NPs at the surface of the grains. The composition and the physicochemical data of the composites $\mathbf{X_{10–40}Au_{5–20}}$ are given in Table 2.

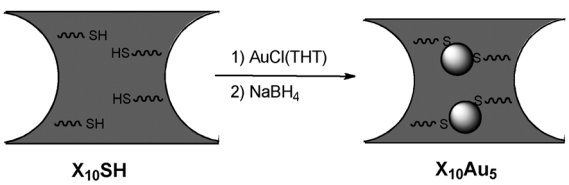

Fig. 7 Growing of AuNPs in $\mathbf{X_{10}SH}$ material.

Table 2 Composition and physicochemical characteristics of the materials $\mathbf{X_{10–40}Au_{5–20}}$

Entry	Material	Au/S [a]	Si/Au [a]	S_{BET} ($m^2\ g^{-1}$)	D_p (nm) [b]	V_p ($cm^3\ g^{-1}$)	d_{100} (nm)
1	$\mathbf{X_{10}Au_5}$	0.287	46.3	250	7.04	0.44	8.48
2	$\mathbf{X_{20}Au_5}$	0.389	65.3	300	6.94	0.52	9.07
3	$\mathbf{X_{40}Au_5}$	0.353	109.8	512.	6.34	0.81	9.74
4	$\mathbf{X_{10}Au_{10}}$	0.202	65.8	389	6.33	0.62	9.07
5	$\mathbf{X_{10}Au_{20}}$	0.131	101.3	403	6.41	0.65	9.23

[a] Ratio calculated from elemental analyses. [b] Calculated from the desorption branch by the BJH method.

The XRD patterns of $\mathbf{X_{10-40}Au_{5-20}}$ revealed that the ordered mesostructure of the host materials survived the loading with AuNPs (see ESI 4†). Furthermore, in all cases, the XRD patterns of the composite materials revealed an increase of the peak intensity of the second and third reflections in comparison with those of the corresponding host materials. Of particular interest was the XRD pattern of $\mathbf{X_{10}Au_5}$ in which the second and third reflections became clearly visible, which was not the case for the original material $\mathbf{X_{10}SH}$. As an example, the XRD pattern of $\mathbf{X_{20}Au_5}$ is shown in Fig. 3. The increase in diffraction intensity probably originates from an increased X-ray scattering contrast between the walls and the pores of the materials, thus demonstrating the location of the AuNPs within the framework of the materials. This same observation was also made by Choi *et al.* after the formation of a uniform polymer coating on the surface of the silica framework.[27] This effect is opposite to that observed after filling the pores with metal ions[28] or nanoparticles.[3,4]

The XRD pattern of $\mathbf{X_{20}Au_5}$ displayed for the high-angle region (2θ = 20–90°) (see inset in Fig. 3) broad reflections at 38.24, 43.81, 64.41 and 78.05° characteristic of gold(0) nanoparticles.

TEM images of $\mathbf{X_{20}Au_5}$ (Fig. 8) show clearly that the mesoscopic order of the host material was maintained in accordance with the XRD results. Furthermore, AuNPs appear as dark dot-like objects outside the channel pores. They are mainly confined within the framework with a uniform size of about 2–3 nm. Based on the Scherrer formula,[29] the average size of AuNPs deduced from the XRD profile of $\mathbf{X_{20}Au_5}$ was found to be 2.0 nm.

Further evidence for the location of the AuNPs within the framework was given in comparing the BET measurements of the $\mathbf{X_{10-40}Au_{5-20}}$ samples with those of the corresponding host materials. The isotherms show clearly an important diminution of the microporosity after growing of NPs (see Fig. 6). In addition, the mesoporosity of the $\mathbf{X_{10-40}Au_{5-20}}$ samples is not very different from that of the host materials. That demonstrates that the pores are not filled by the NPs and remain empty. These observations constitute additional evidence for the location of NPs in the framework.

The size of NPs was found to depend slightly on the percentage of organic groups in the framework. The NPs become very small (<2 nm) in $\mathbf{X_{40}Au_5}$, while for the more concentrated material in SH groups $\mathbf{X_{10}Au_{20}}$, the NP size is no more monodisperse (see ESI 5†).

Finally, it is worth noting that, when starting from the materials $\mathbf{X_{10-40}2}$ in which the framework is functionalized with SS groups or from pure **SBA-15** silica, there is no control of the location or the size of AuNPs. This clearly appears on the corresponding TEM images (see ESI 6†).

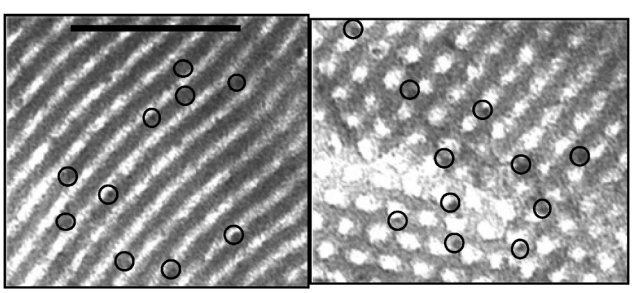

Fig. 8 TEM images of $\mathbf{X_{20}Au_5}$. Scale bar: 50 nm.

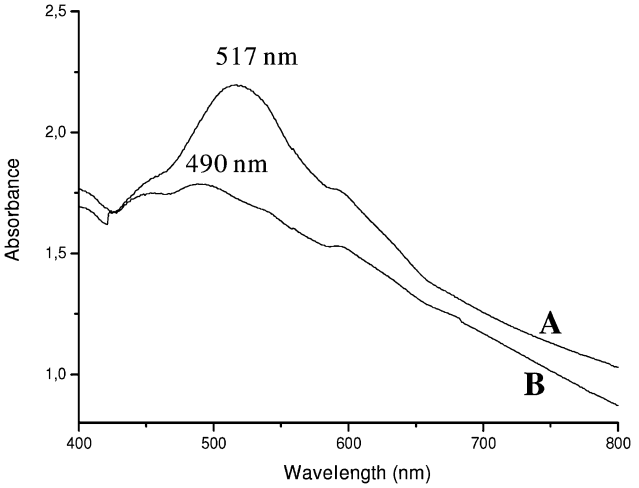

Fig. 9 UV-visible spectra for composite materials **AuNPs-SBA-15** (A) and $\mathbf{X_{40}Au_5}$ (B).

Fig. 9 shows the UV-visible spectra of composite materials **AuNPs-SBA-15** silica (A) and $\mathbf{X_{40}Au_5}$ (B). The λ_{max} values were obtained at 517 nm and 490 nm respectively. The blue shift of 27 nm observed for $\mathbf{X_{40}Au_5}$ is in accordance with the small size of nanoparticles (~2 nm).[30]

Thus, the functionalisation of the framework of mesoporous materials with an appropriate organic group appears to be the key factor controlling the location of NPs.

The role of the organic moieties was further highlighted by heating the materials $\mathbf{X_{10-40}Au_{5-20}}$. Indeed, we have observed that the AuNPs are stable as long as the organic groups remain intact, that is to say up to about 200 °C. Beyond this temperature, TG analysis reveals that there is loss of organic moieties which involves the sintering of AuNPs (see ESI 7†).

Conclusions

We have described a methodology allowing the confinement of monodisperse gold nanoparticles (AuNPs) of small size (~2 nm) in the framework of mesoporous organosilica. Our approach is based on the functionalisation of the framework of mesoporous organosilica with SH groups, followed by the impregnation/reduction of AuCl(THT) as an organometallic precursor of AuNPs. We have shown that the functionalisation of the framework of mesoporous materials with an appropriate organic group is the key factor allowing the formation of monodisperse NPs located in the walls of the materials. The generalization of the method to other NPs is expected following adaptation of the functionalisation of the walls to the NPs chosen. This methodology could open the way to materials containing two kinds of NPs perfectly located at nanometric scale, one in the channel pores, and the other in the framework.

Acknowledgements

The authors thank Dr Arie van der Lee (IEM, Montpellier, France) for XRD measurements, and the CNRS and Montpellier University for financial support.

References

1 *Nanoparticles: From Theory to Applications*, ed. G. Schmid, Wiley-VCH, Weinheim, 2004; K. Philippot and B. Chaudret, *C. R. Chim.*, 2003, **6**, 1019; B. Chaudret, *Top. Organomet. Chem*, 2005, **16**, 233.
2 (*a*) D. Ozkaya, W. Zhou, J. M. Thomas, P. Midgley, V. J. Keast and S. Hermans, *Catal. Lett.*, 1999, **60**, 113; (*b*) F. Schweyer, P. Braunstein, C. Estournès, J. Guille, H. Kessler, H.-L. Paillaud and J. Rosé, *Chem. Commun.*, 2000, 1271; (*c*) Z. Y. Yuan, S. Q. Liu, T. H. Chen, J. Z. Wang and H. X. Li, *Chem. Commun.*, 1995, 973; (*d*) Y. Plyuto, J.-M. Berquier, C. Jacquiod and C. Ricolleau, *Chem. Commun.*, 1999, 1653; (*e*) P. Mukherjee, C. R. Patra, R. Kumar and M. Sastry, *Phys. Chem. Commun.*, 2001, **5**; (*f*) C. R. Patre, A. Ghosh, P. Mukherjee, M. Sastry and R. Kumar, *Stud. Surf. Sci. Catal.*, 2002, **141**, 641; (*g*) T. Abe, Y. Tachibana, T. Uematsu and M. Iwamoto, *J. Chem. Soc., Chem. Commun.*, 1995, 1617; (*h*) M. Iwamoto, T. Abe and Y. Tachibana, *J. Mol. Catal. A: Chem.*, 2000, **155**, 143; (*i*) R. S. Mulukutla, K. Asakura, S. Namba and Y. Iwasawa, *Chem. Commun.*, 1998, 1425; (*j*) M. Fröba, R. Köhn, G. Bouffaud, O. Richard and G. van Tendeloo, *Chem. Mater.*, 1999, **11**, 2858; (*k*) A. Fukuoka, M. Osada, T. Shido, S. Inagaki, Y. Fukushima and M. Ichikawa, *Inorg. Chim. Acta*, 1999, **294**, 281; (*l*) H. Fukuoka, Y. Araki, N. Sakamoto, H. Sugimoto, Y. Tsukoda, Y. Kumai, Akimoto and M. Ichikawa, *Nano Lett.*, 2002, **2**, 793; (*m*) W. Zhu, Y. Han and L. An, *Micropor. Mesopor. Mater.*, 2005, **80**, 221; (*n*) M. H. Huang, A. Choudrey and P. Yang, *Chem. Commun.*, 2000, 1063.
3 (*a*) C.-M. Yang, P.-H. Liu, Y.-F. Ho, C.-Y. Chiu and K.-J. Chao, *Chem. Mater.*, 2003, **15**, 275; (*b*) J. Gu, J. Lin, G. You, L. Xiong, S. Qian, Z. Hua and H. Chen, *Adv. Mater.*, 2005, **17**, 557; (*c*) Y. Zhao, Y. Qi, S. Zhang and Z. Liu, *Mater. Lett.*, 2008, **62**, 1197; (*d*) X. Zhao, J. Shi, B. Hu, L. Zhang and Z. Hua, *Mater. Lett.*, 2004, **58**, 2152; (*e*) Y. Shan and L. Gao, *Mater. Chem. Phys.*, 2005, **89**, 412; (*f*) J. Gu, J. Shi, G. You, L. Xiong, S. Qian, Z. Hua and H. Chen, *Adv. Mater.*, 2005, **17**, 557.
4 (*a*) Y. Guari, C. Thieuleux, A. Mehdi, C. Reye, R. J. P. Corriu, S. Gomez-Gallardo, K. Philippot and B. Chaudret, *Chem. Mater.*, 2003, **15**, 2017; (*b*) S. Jansat, K. Pelzer, J. Garcia-Anton, R. Raucoules, K. Philippot, A. Maisonnat, B. Chaudret, Y. Guari, A. Mehdi, C. Reyé and R. J. P. Corriu, *Adv. Funct. Mater.*, 2007, **17**, 3339.
5 C. Garcia, Y. Zhang, F. DiSalvo and U. Wiesner, *Angew. Chem., Int. Ed.*, 2003, **42**, 1526.
6 I. Yuranov, L. Kiwi-Minsker, P. Buffat and A. Renken, *Chem. Mater.*, 2004, **16**, 760.
7 C.-M. Yang, H.-A. Lin, B. Zibrowius, B. Spliethoff, F. Schüth, Sz.-C. Liou, M.-W. Chu and C. H. Chen, *Chem. Mater.*, 2007, **19**, 3205.
8 L. Chen, J. Hu and R. Richards, *J. Am. Chem. Soc.*, 2009, **131**, 914.
9 (*a*) S. Inagaki, S. Guan, Y. Fukushima, T. Oshuna and O. Terasaki, *J. Am. Chem. Soc.*, 1999, **121**, 9611; (*b*) B. J. T. Melde, B. Holland, C. F. Blanford and A. Stein, *Chem. Mater.*, 1999, **11**, 3302; (*c*) T. Asefa, M. J. MacLachlan, N. Coombs and G. A. Ozin, *Nature*, 1999, **402**, 867; (*d*) C. Yoshina-Ishii, T. Asefa, N. Coombs, M. J. MacLachlan and G. A. Ozin, *Chem. Commun.*, 1999, 2539.
10 A. Vinu, K. Z. Hossain and K. Ariga, *J. Nanosci. Nanotechnol.*, 2005, **5**, 347.
11 (*a*) F. Hoffmann, M. Cornelius, J. Morell and M. Fröba, *J. Nanosc. Nanotech*, 2006, **6**, 265; (*b*) F. Hoffmann, M. Cornelius, J. Morell and M. Fröba, *Angew. Chem., Int. Ed.*, 2006, **45**, 3216.
12 S. S. Park and C. S. Ha, *Chem. Rec.*, 2006, **6**, 32.
13 S. Fujita and S. Inagaki, *Chem. Mater.*, 2008, **20**, 891.
14 Q. Yang, J. Liu, L. Zhang and C. Li, *J. Mater. Chem.*, 2009, DOI: 10.1039/b815012e.
15 M. C. Burleigh, M. A. Markowitz, M. S. Spector and B. P. Gaber, *Chem. Mater.*, 2001, **13**, 4760.
16 M. Benitez, D. Das, R. Ferreira, U. Pischel and H. Garcia, *Chem. Mater.*, 2006, **18**, 5597.
17 J. Liu, J. Yang, Q. Yang, G. Wang and Y. Li, *Adv. Funct. Mater.*, 2005, **15**, 1297.
18 J. Liu, Q. Yang, L. Zhang, D. Jiang, X. Shi, J. Yang, H. Zhong and C. Li, *Adv. Funct. Mater.*, 2007, **17**, 569.
19 O. Kwon, S. Park and G. Seo, *Chem. Commun.*, 2007, 4113.
20 T. Hayashi, K. Tanaka and M. Haruta, *J. Catal.*, 1998, **178**, 566.
21 R. Uson, A. Laguna and M. Laguna, *Inorg. Synth.*, 1989, **26**, 85.
22 J. Alauzun, A. Mehdi, C. Reyé and R. J. P. Corriu, *J. Am. Chem. Soc.*, 2006, **128**, 8718.
23 O. Olkhovyk and M. Jaroniec, *J. Am. Chem. Soc.*, 2005, **127**, 60.
24 H. Zhu, D. J. Jones, J. Zajac, R. Dutartre, M. Rhomari and J. Rozière, *Chem. Mater.*, 2002, **14**, 4886.
25 L. E. Overman, J. Smoot and J. D. Overman, *Synthesis*, 1974, 59.
26 A. C. Templeton, W. P. Wuelfing and R. W. Murray, *Acc. Chem. Res.*, 2000, **33**, 27.
27 M. Choi, F. Kleitz, D. Liu, H. Y. Lee, W.-S. Ahn and R. Ryoo, *J. Am. Chem. Soc.*, 2005, **127**, 1924.
28 R. J. P. Corriu, E. Lancelle-Beltran, A. Mehdi, C. Reye, S. Brandes and R. Guilard, *J. Mater. Chem.*, 2002, **12**, 1355.
29 Scherrer formula: $d = k\lambda/\beta_{1/2}\cos\theta$, where k is the coefficient taken as 0.9, λ is the wavelength of X-ray radiation and $\beta_{1/2}$ is the full-width half-maximum linewidth in radians.
30 P. K. Jain, X. Huang, I. H. El-Sayed and M. A. El-Sayed, *Acc. Chem. Res.*, 2008, **41**, 1578.

